Acta Physica Polonica B Proceedings Supplement **17**, 7-A7 (2024)

STUDY OF DEFECTS IN TiO_2 POLYMORPHS USING POSITRON ANNIHILATION*

Oksana Melikhova, Jakub Čížek, Dejan Prokop
František Lukáč

Faculty of Mathematics and Physics, Charles University
V Holešovičkách 2, 180 00 Praha 8, Czech Republic

Received 19 July 2024, accepted 9 October 2024,

This work presents a comparative study of point defects in three TiO_2 polymorphs: anatase, rutile, and brookite. Open volume point defects were characterized using the positron annihilation spectroscopy combined with *ab initio* calculations of positron lifetimes. The TiO_2 polymorphs have been investigated in the form of polycrystalline powders and nanopowders. Polycrystalline and nanocrystalline TiO_2 powders contain vacancies, vacancy clusters, and nanoscopic pores in which positronium forms. Anatase has the most open structure and exhibits the longest positron lifetimes. In contrast, the shortest positron lifetimes were observed for rutile.

DOI:10.5506/APhysPolBSupp.17.7-A7

1. Introduction

Titanium dioxide (TiO_2) is a photocatalytic material that facilitates environmentally important chemical reactions such as the splitting of water to produce hydrogen [1]. At atmospheric pressure, TiO_2 naturally occurs in three polymorphs: rutile (tetragonal), anatase (tetragonal), and brookite (orthorhombic). While rutile is the stable phase, both anatase and brookite are metastable and transform irreversibly to rutile at elevated temperatures [2]. Both rutile and anatase have distinct properties that make them suitable for various medical applications, particularly in areas such as drug delivery [3, 4], antibacterial coatings [5], and biosensing [6]. Anatase is recognized for its superior photocatalytic activity compared to rutile, making it valuable for applications in environmental remediation and antibacterial surfaces. The photocatalytic mechanism involves generating reactive oxygen species that can disinfect surfaces and reduce bacterial load, which is crucial

---

[*] Presented at the 5th Jagiellonian Symposium on *Advances in Particle Physics and Medicine*, Cracow, Poland, June 29–July 7, 2024.

in preventing device-related infections and combating antibiotic-resistant bacteria [6]. Rutile is used in the development of biomedical implants due to its biocompatibility and low allergenicity [7].

Since functional properties, *e.g.* catalytic activity of TiO_2, are strongly influenced by point defects [8], it is important to characterize point defects in TiO_2. The positron annihilation spectroscopy (PAS) [9] using positron or positronium (Ps) [10] as a probe of open-volume defects is a powerful tool for defect studies in solids. PAS has been employed for the characterization of point defects in rutile [11] and anatase [12]. However, no comparative PAS study of open volume point defects in TiO_2 polymorphs has been done so far. This work presents the results of PAS characterization of open-volume point defects in rutile, anatase, and brookite.

2. Experimental

The TiO_2 polymorphs were investigated in the form of polycrystalline and nanocrystalline powders prepared by sol-gel synthesis. The investigated samples are described in Table 1.

Table 1. List of samples studied. Polycrystalline powders have grain size of the order of 10 μm, nanopowders have grain size smaller than 100 nm. The last column shows lattice parameters determined by XRD.

Sample	Description	Phase	Lattice parameters [Å]
R-POLY	polycrystalline powder Merck 204730	rutile	$a = 4.59510(1)$ $c = 2.95965(1)$
R-NANO	nanopowder Merck 637262	rutile	$a = 4.5968(1)$ $c = 2.9596(1)$
A-POLY	polycrystalline powder Merck 2322033	anatase	$a = 3.78634(2)$ $c = 9.51731(6)$
B-NANO	nanopowder Merck 791326	brookite	$a = 5.1370(2)$ $b = 5.4519(2)$ $c = 9.1766(4)$

The phase composition of samples was determined by X-ray diffraction (XRD) using CuK_α radiation and a Bruker D8 Discover diffractometer with the 1D Lynx-Eye detector. The lattice parameters and phase composition were determined by Rietveld analysis of XRD patterns using `TOPAS V5` code [13].

A ^{22}Na radioisotope with activity of 1 MBq deposited on a 7 μm Kapton foil was used as a positron source. It was placed in the center of a cylindrical chamber with the diameter of 10 mm and height of 5 mm filled with measured powder so that all positrons emitted from the source are stopped in the measured powder. The chamber was completely filled with the measured powder and sealed. No external pressure was applied, and the chamber was not evacuated. The loose powders were measured under atmospheric pressure. The positron lifetime measurements were carried out using a digital spectrometer [14] with the time resolution of 145 ps (FWHM of resolution function). At least 10^7 positron annihilation events were collected in each positron lifetime spectrum. The source contribution consisting of a component with the lifetime of 380 ps and intensity of 10% was determined using a procedure described in Ref. [15], and was always subtracted from positron lifetime spectra. Decomposition of positron lifetime spectra into individual components was done using a PLRF19 code [16].

3. Theoretical modeling

Positron lifetimes were calculated within the two-component density functional theory using the so-called standard scheme [17] and employing the code described in Refs. [18, 19]. First, the electron density $n_-(\boldsymbol{r})$ in the crystal without positron was calculated. Subsequently, the ground-state positron wave function $\psi_+(\boldsymbol{r})$ and the energy eigenvalue E_+ were calculated by solving the single-particle Schrödinger equation

$$-\frac{1}{2}\nabla^2\psi_+(\boldsymbol{r}) + V_+(\boldsymbol{r})\psi_+(\boldsymbol{r}) = E_+\psi_+(\boldsymbol{r})$$

for positron in an effective potential

$$V_+(\boldsymbol{r}) = \phi(\boldsymbol{r}) + V_{xc}[n_-]$$

consisting of the Coulomb potential $\phi(\boldsymbol{r})$ produced by the charge distribution of electrons and nuclei and the electron–positron exchange-correlation functional $V_{xc}[n_-]$ in the limit of vanishing positron density [17]. The positron lifetime τ was calculated as the inverse of the overlap integral of the electron density $n_-(\boldsymbol{r})$ and positron density $n_+(\boldsymbol{r}) = |\psi_+(\boldsymbol{r})|^2$ using the equation

$$\tau = \left\{\pi r_e^2 c \int n_-(\boldsymbol{r}) n_+(\boldsymbol{r}) \gamma[n_-]\, \mathrm{d}\boldsymbol{r}\right\}^{-1},$$

where r_e and c stand for the classical electron radius and the speed of light, respectively. The enhancement factor $\gamma[n_-]$ accounts for an increase in the electron density at the site of the positron [17]. We used the local density approximation of $\gamma[n_-]$ and $V_{xc}[n_-]$ parametrized by Boroński and Nieminen [20] with a correction for incomplete positron screening in semiconductors [21].

The tetragonal structure (space group $P4_2/mnm$) with lattice parameters $a = 4.596$ Å and $c = 2.960$ Å was considered for rutile. Point defects were modeled using $4\times4\times4$ supercell (128 Ti and 256 O atoms). In the case of anatase the calculations were done using the tetragonal structure (space group $I4_1/amd$) with lattice parameters $a = 3.786$ Å and $c = 9.517$ Å. Defects were modeled using $4 \times 4 \times 4$ supercell (256 Ti and 512 O atoms). The orthorombic structure (space group Pbca) with lattice parameters $a = 5.1371$ Å, $b = 5.4521$ Å, and $c = 9.1774$ Å was considered for brookite. Defects were modeled using $4 \times 4 \times 4$ supercell (512 Ti and 1024 O atoms). Ion relaxations were not considered. Convergence tests with respect to the supercell size showed that calculated positron lifetimes are converged within 0.1 ps.

4. Results

Table 2 shows the calculated lifetimes of positrons annihilated in the free state (bulk) and trapped at various defects in the three TiO_2 polymorphs. The following defects were considered for each phase: oxygen vacancy (V_O), titanium vacancy (V_{Ti}), titanium and oxygen divacancy ($V_{Ti} + V_O$), and $V_{Ti} + 2V_O$ complex consisting of V_{Ti} and two V_O in the nearest neighbor sites, *i.e.* missing TiO_2 unit. The calculated positron binding energy for each defect is included in Table 2 as well. The bulk positron lifetimes for the three TiO_2 polymorphs are significantly different. Anatase has the most open structure reflected by the longest bulk positron lifetime, while rutile has the shortest bulk positron lifetime. Figure 1 (a) shows that the bulk positron lifetime linearly increases with increasing cell volume per TiO_2 unit.

Table 2. Calculated lifetimes of free positrons (bulk) and positrons trapped at various defects in the three TiO_2 polymorphs. The calculated positron binding energies E_B for various defects are listed in the table as well.

	Rutile		Anatase		Brookite	
	τ [ps]	E_B [eV]	τ [ps]	E_B [eV]	τ [ps]	E_B [eV]
bulk	144	—	174	—	156	—
V_O	146	0.02	175	0.01	158	0.01
V_{Ti}	168	1.25	184	0.58	173	0.96
$V_{Ti} + V_O$	191	1.60	208	0.88	199	1.32
$V_{Ti} + 2V_O$	211	1.89	232	1.14	214	1.53

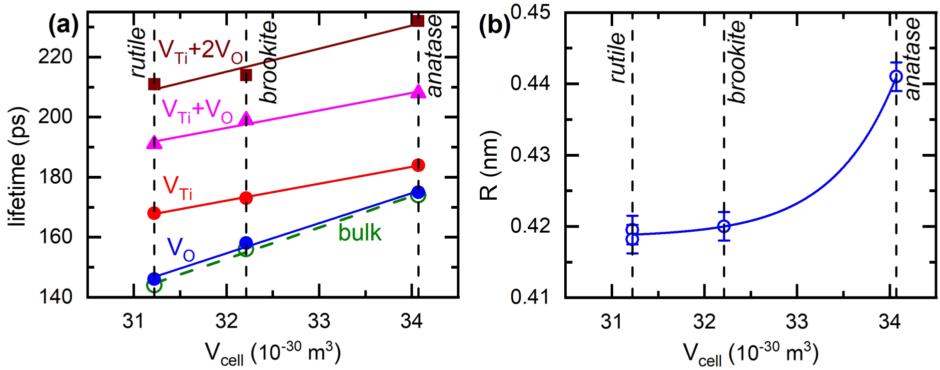

Fig. 1. (a) Calculated positron lifetimes plotted as a function of the cell volume per $\mathrm{TiO_2}$ unit; (b) the mean radius of nanoscopic pores in the $\mathrm{TiO_2}$ powder samples.

The positron lifetimes calculated for V_{O} are very close to the bulk positron lifetimes and positron binding energies to V_{O} are negligible. Hence, V_{O} are too shallow potential wells incapable of positron confinement and V_{O} are "invisible" for positrons. On the other hand, V_{Ti} is a deep positron trap with positron binding energy of 0.58–1.25 eV depending on the polymorph. The calculated lifetime of positrons trapped in V_{Ti} is significantly longer than the bulk positron lifetime and also linearly increases with the cell volume. $V_{\mathrm{Ti}} + V_{\mathrm{O}}$ and $V_{\mathrm{Ti}} + 2V_{\mathrm{O}}$ complexes are even deeper potential wells and the calculated positron lifetimes are further prolonged. Similarly to V_{Ti}, the lifetime of trapped positrons linearly increases with the cell volume per $\mathrm{TiO_2}$ unit.

The positron lifetime spectra measured in all $\mathrm{TiO_2}$ powder samples can be well described by three components summarized in Table 3. The lifetimes of all components are higher than the corresponding bulk lifetimes. It indicates that concentration of defects in the powders is so high that

Table 3. Results of the positron lifetime measurements for $\mathrm{TiO_2}$ powders: lifetimes τ_i and relative intensities I_i of the components resolved in the positron lifetime spectra.

Sample	τ_1 [ps]	I_1 [%]	τ_2 [ps]	I_2 [%]	τ_3 [ns]	I_3 [%]
R-POLY	178(3)	38(1)	354(3)	60(1)	3.8(1)	2(1)
R-NANO	215(4)	39(2)	397(4)	58(2)	3.82(7)	3(1)
A-POLY	200(10)	10(1)	372(2)	88(1)	4.2(1)	2(1)
B-NANO	229(3)	21(2)	423(3)	76(2)	3.83(8)	3(1)

all positrons are trapped at defects. The first component with lifetime τ_1 can be attributed to vacancy-like defects. The lifetime τ_1 is close to the lifetimes calculated for $V_{Ti} + V_O$ or $V_{Ti} + 2V_O$ complexes. Hence, the component τ_1 comes from positrons trapped at V_{Ti} which are likely associated with one or two V_O. The longer component with lifetime τ_2 comes from positrons trapped at large defects, namely the vacancy clusters corresponding to several missing Ti and O ions. High intensity I_2 of this component indicates that the vacancy clusters represent the dominating type of defects in polycrystalline and nanocrystalline powders. The long-lived component with lifetime τ_3 comes from the pick-off annihilation of ortho-positronium (oPs) formed inside internal cavities [10]. The presence of this component confirms that TiO_2 powder samples contain nanoscopic pores. Supposing that the nanoscopic pores have a spherical shape, their mean radius, R, can be estimated from the lifetime τ_3 using the Tao–Eldrup model [22, 23]. Figure 1 (b) shows that mean pore radius R increases approximately exponentially with the cell volume per TiO_2 unit.

Note that some positrons can diffuse to the grain surface and form Ps by picking up an electron on the surface. The Ps atom formed on the surface is then emitted into the free space among the grains. To estimate the fraction of positrons that can reach the grain surface by diffusion, let us consider a polycrystalline powder with a mean grain size $d \approx 10$ μm. The mean positron diffusion length in defect-free semiconductors is typically in the range of 100 nm [24]. However, the powders studied in our experiment contain a very high concentration of defects, as evidenced by saturated positron trapping. Therefore, the actual positron diffusion length L_+ in the measured powders is shortened down to an order of magnitude lower value, around 10 nm. The fraction f of positrons that can reach the grain surface by diffusion within a grain is determined by the ratio of the volume of the sub-surface region with a thickness of t_s to the net volume of the grain, $f = \pi d^2 t_s / \frac{1}{6}\pi d^3 = 6t_s/d$. Assuming that positrons can reach the surface by diffusion from a sub-surface layer with a thickness of $t_s \approx 3L_+ \approx 30$ nm, one gets a fraction of 2% of positrons diffusing to the grain surface. Nanocrystalline powders are made up of grains that are around 100 nm in size. However, these nanocrystalline grains are clumped together into particles that consist of several grains. The average size of these particles is similar to the grain size of polycrystalline powders. Therefore, in nanocrystalline powders, the fraction of positrons that reach the surfaces of particles and form Ps there is comparable to that in polycrystalline powders.

However, since we measure loose powders, the size of free volumes among particles is comparable to the particle size, *i.e.* it is of the order of a few μm. In these large open volumes, o-Ps is predominantly annihilated by three-gamma self-annihilation, resulting in annihilation photons with energy lower than 511 keV, which does not match the energy window of the spectrometer adjusted to the energy of 511 keV. As a result, the three-gamma annihilations are not visible in the present experiment. Additionally, the o-Ps lifetime in the micron-size free volumes among particles approaches the vacuum value of 142 ns, which is two orders of magnitude higher than the lifetimes measured for our powders. This indicates that the o-Ps lifetimes listed in Table 3 correspond to the two-gamma pick-off annihilation of o-Ps localized in small nanoscopic pores inside powder particles.

5. Conclusions

Positron lifetimes for different TiO_2 polymorphs are significantly different and linearly increase with the cell volume per TiO_2 unit. Polycrystalline and nanocrystalline powders of all TiO_2 polymorphs contain vacancy clusters as a dominating type of defects and, in addition, also nanoscopic pores in which positronium is formed. The mean size of nanoscopic pores exponentially increases with the cell volume per TiO_2 unit.

This work was supported by the Czech Science Foundation (project 22-21547S). Computational resources for *ab initio* calculations were supplied by the e-INFRA CZ project (ID:90140), supported by the Ministry of Education, Youth and Sports of the Czech Republic.

REFERENCES

[1] O. Carp, C.L. Huisman, A. Reller, *Prog. Solid State Chem.* **32**, 33 (2004).

[2] D.A.H. Hanaor, C.C. Sorrell, *J. Mater. Sci.* **46**, 855 (2011).

[3] N. Thakur *et al.*, *Sci. Total Environ.* **914**, 169815 (2024).

[4] S. Lawrence, W.A. James, S. Stewart, *Brit. J. Pharm.* **8**, 1349 (2023).

[5] C.-J. Chung *et al.*, *J. Biomed. Mater. Res. B* **85**, 220 (2008).

[6] S. Jafari *et al.*, *Int. J. Nanomedicine* **15**, 3447 (2020).

[7] P.-I. Branemark, *J. Prosthet. Dent.* **50**, 399 (1983).

[8] H. Zhao, F. Pan, Y. Li, *J. Materiomics* **3**, 17 (2017).

[9] J. Čížek, *J. Mater. Sci. Technol.* **34**, 577 (2018).

[10] D.W. Gidley, H.-G. Peng, R.S. Vallery, *Annu. Rev. Mater. Res.* **36**, 49 (2006).

[11] R.V. Nair *et al.*, *J. Phys. D: Appl. Phys.* **51**, 045107 (2018).

[12] S. Ghosh, P.M.G. Nambissan, *J. Solid State Chem.* **275**, 174 (2019).

[13] A.A. Coelho, *J. Appl. Cryst.* **51**, 210 (2018).

[14] F. Bečvář, J. Čížek, I. Procházka, J. Janotová, *Nuclear Instrum. Methods Phys. Res. A* **539**, 372 (2005).

[15] J. Čížek *et al.*, *Materialia* **23**, 101450 (2022).

[16] J. Čížek, *Acta Phys. Pol. A* **137**, 177 (2020).

[17] M.J. Puska, R.M. Nieminen, *Rev. Mod. Phys.* **66**, 841 (1994).

[18] J. Kuriplach, C. Dauwe, D. Segers, M. Šob, *Nukleonika* **42**, 143 (1997).

[19] J. Kuriplach *et al.*, *Phys. Rev. B* **58**, 10475 (1998).

[20] E. Boroński, R.M. Nieminen, *Phys. Rev. B* **34**, 3820 (1986).

[21] M.J. Puska, S. Mäkinen, M. Manninen, R.M. Nieminen, *Phys. Rev. B* **39**, 7666 (1989).

[22] S.J. Tao, *J. Chem. Phys.* **56**, 5499 (1972).

[23] M. Eldrup, D. Lightbody, J.N. Sherwood, *Chem. Phys.* **63**, 51 (1981).

[24] C. Hugenschmidt, *Surf. Sci. Rep.* **71**, 547 (2016).